Acta Cryst. (1999). B**55**, 1014–1029

Order–disorder phenomena determined by high-resolution powder diffraction: the structures of tetrakis(trimethylsilyl)methane $C[Si(CH_3)_3]_4$ and tetrakis(trimethylsilyl)silane $Si[Si(CH_3)_3]_4$

Robert E. Dinnebier,[a]* Wayne A. Dollase,[b] Xavier Helluy,[c] Jörg Kümmerlen,[d] Angelika Sebald,[d] Martin U. Schmidt,[e] Silvina Pagola,[f] Peter W. Stephens[f] and Sander van Smaalen[a]

[a]*Laboratory of Crystallography, University of Bayreuth, D-95440 Bayreuth, Germany,* [b]*ESS Department, University of California, Los Angeles, CA 90095, USA,* [c]*Rhône-Poulenc Rorer, Department of Pharmaceutical Sciences, Preformulation/Physical Analysis, Research Center of Vitry-Alfortville, 13 quai Jules Guesde, BP 14, 94403 Vitry sur Seine CEDEX, France,* [d]*Bayerisches Geoinstitut, University of Bayreuth, D-95440 Bayreuth, Germany,* [e]*Clariant GmbH, Pigment Technology Research, G834, D-65926 Frankfurt am Main, Germany, and* [f]*Department of Physics and Astronomy, SUNY at Stony Brook, Stony Brook, NY 11794-3800, USA.*
E-mail: robert.dinnebier@uni-bayreuth.de

(*Received 10 November 1998; accepted 30 April 1999*)

Abstract

The compounds tetrakis(trimethylsilyl)methane $C[Si(CH_3)_3]_4$ (TC) and tetrakis(trimethylsilyl)silane $Si[Si(CH_3)_3]_4$ (TSi) have crystal structures with the molecules in a cubic closed-packed (c.c.p.) stacking. At room temperature both structures have space group $Fm\bar{3}m$ ($Z = 4$) with $a = 13.5218$ (1) Å, $V = 2472.3$ (1) Å^3 for TSi, and $a = 12.8902$ (2) Å, $V = 2141.8$ (1) Å^3 for TC. X-ray scattering data can be described by a molecule with approximately sixfold orientational disorder, ruling out a structure with free rotating molecules. Upon cooling, TSi exhibits a first-order phase transition at $T_c = 225$ K, as is characterized by a jump of the lattice parameter of $\Delta a = 0.182$ Å and by an exothermal maximum in differential scanning calorimetry (DSC) with $\Delta H = 11.7$ kJ mol^{-1} and $\Delta S = 50.0$ J mol^{-1} K^{-1}. The structure of the low-temperature phase is refined against X-ray powder data measured at 200 K. It has space group $P2_13$ ($Z = 4$), $a = 13.17158$ (6) Å and $V = 2285.15$ (2) Å^3. The molecules are found to be ordered as a result of steric interactions between neighboring molecules, as is shown by analyzing distances between atoms and by calculations of the lattice energy in dependence on the orientations of the molecules. TC has a phase transition at $T_{c1} = 268$ K, with $\Delta a_1 = 0.065$ Å, $\Delta H_1 = 3.63$ kJ mol^{-1} and $\Delta S_1 = 13.0$ J mol^{-1} K^{-1}. A second first-order phase transition occurs at $T_{c2} = 225$ K, characterized by $\Delta a_2 = 0.073$ Å, $\Delta H_2 = 6.9$ kJ mol^{-1} and $\Delta S_2 = 30.0$ J mol^{-1} K^{-1}. The phase transition at higher temperature has not been reported previously. New NMR experiments show a small anomaly in the temperature dependence of the peak positions in NMR to occur at T_{c2}. Rietveld refinements were performed for the low-temperature phase measured at $T = 150$ K [space group $P2_13$, lattice parameter $a = 12.609$ (3) Å], and for the intermediate phase measured at $T = 260$ K [space group $Pa\bar{3}$, lattice parameter $a = 12.7876$ (1) Å]. The low-temperature phase of TC is formed isostructural to the low-temperature phase of TSi. In the intermediate phase the molecules exhibit a twofold orientational disorder.

1. Introduction

Tetrakis(trimethylsilyl)methane, $C[(Si(CH_3)_3]_4$ (TC), and tetrakis(trimethylsilyl)silane, $Si[Si(CH_3)_3]_4$ (TSi), form non-polar almost spherically shaped molecules which may be viewed as small fragments of a diamond-like tetrahedral structure terminated by a shell of H

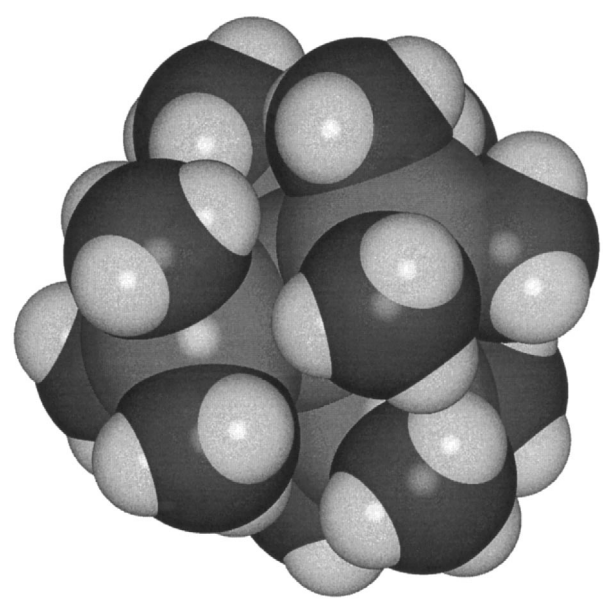

Fig. 1. Cup model of molecules $C[Si(CH_3)_3]_4$ (TC) and $Si[Si(CH_3)_3]_4$ (TSi) in the low-temperature phase showing the quasi-spherical shape.

ISSN 0108-7681

atoms (Fig. 1). Solid-state NMR studies (Dereppe & Magill, 1972; Aliev *et al.*, 1993, 1994; Helluy *et al.*, 1998) have established that at room temperature the molecules in crystalline TC and TSi undergo rapid (kHz scale) reorientational jumps about fixed centers of mass forming so-called 'rotator-phases' or 'plastic' crystals (Parsonage & Staveley, 1978). Upon cooling, these crystalline solids undergo phase transitions to structures of increasing order, as evidenced by NMR and scanning calorimetry measurements (Murrill & Breed, 1971; Dereppe & Magill, 1972; Aliev *et al.*, 1993, 1994; Helluy *et al.*, 1998). TC and TSi belong to a class of molecules with the general formula $M^1(M^2X_3)_4$, where M^1, M^2 = C, Si, Ge, Sn and X = CH_3, Br, Cl, . . . (Bürger & Goetze, 1968; Kuivila & DiStefano, 1976; Klinkhammer *et al.*, 1995; Haaland *et al.*, 1996, 1997; Matsunaga *et al.*, 1995).

The molecular structures of TC and TSi in the gas phase have been determined by electron diffraction (Bartell *et al.*, 1970; Beagley *et al.*, 1988, 1989). In the gas phase both molecules have 23(T) symmetry, with small ($\sim$18° for TC, $\sim$14° for TSi) cooperative twisting of the trimethylsilyl groups from a fully extended staggered T_d configuration to reduce steric hindrance between methyl groups (Fig. 1). These conformations have been corroborated by force-field calculations (Iroff & Mislow, 1978; Beagley *et al.*, 1988). This high symmetry is retained in the solid state at room temperature. The molecular symmetry is reduced to 3(C_3) in the low-temperature phases of both compounds, as was inferred from qualitative consideration of ^{13}C and ^{29}Si MAS NMR experiments (Aliev *et al.*, 1993, 1994). More recently it was confirmed by a quantitative analysis of one- and two-dimensional variable-temperature ^{13}C and ^{29}Si MAS NMR experiments on TC and TSi (Helluy *et al.*, 1998).

The synthesis of TC and TSi was reported as early as 1964 (Merker & Scott, 1964; Gilman & Smith, 1964), but single crystals of TC and TSi have remained unavailable. Crystals have been grown for two thf adducts TSi.thf and TSi·$[(Me_3Si)_3SiLi(thf)_3]_2$ (Heine *et al.*, 1993). Crystalline powder of solvent-free TC has been studied previously by X-ray powder diffraction at room temperature (Merker & Scott, 1964; Dereppe & Magill, 1972). A face-centered cubic lattice [lattice parameter a = 12.90 (1) Å] and an observed density of 0.9113 g cm^{-3} were reported, consistent with a cubic close-packed array (Z = 4) of statistically disordered rotator molecules.

Here we report the structure determinations of the solid-state structures of TC and TSi at several temperatures from X-ray powder diffraction and solid-state NMR data. Furthermore, the occurrence of an additional intermediate low-temperature phase for TC is identified by high-resolution X-ray powder diffraction and DSC measurements. The intermolecular interactions of the low-temperature phases of TC and TSi are investigated by force-field calculations of the lattice energy.

2. Experimental

TSi is commercially available (ABCR Chemicals, Karlsruhe, Germany) and has been used without further purification. Neither ^{1}H solution- and ^{13}C, ^{29}Si solid-state NMR nor preliminary laboratory X-ray analysis revealed impurities. Our sample of TC was kindly donated by G. Fritz, Karlsruhe. The polycrystalline samples consisted of fine equidimensional colorless grains without discernible crystal faces. They are stable in air. Owing to the softness of the material, grinding of the sample was not possible and a razor blade was used instead to produce a finely powdered sample.

Differential scanning calorimetry (DSC) was performed for both compounds between 298 and 153 K on a TA Instruments Modulated Differential Scanning 2920 calorimeter, equipped with a liquid-nitrogen cooling device and Universal Analysis Software (a cooling rate of 1 K min^{-1} and a temperature-modulation amplitude of 2 K min^{-1} was used). The DSC data for TC indicate phase transitions at T = 279 K (ΔH_1 = 3.63 kJ mol^{-1}, ΔS_1 = 13.0 J mol^{-1} K^{-1}) and T = 227 K (ΔH_2 = 6.9 kJ mol^{-1}, ΔS_2 = 30.0 J mol^{-1} K^{-1}; Fig. 2*a*). The transition at T = 279 K has not been mentioned in an earlier calorimetry study on TC (Dereppe & Magill, 1972). For TSi the thermogram indicates a single phase transition at T = 231 K (ΔH = 11.7 kJ mol^{-1}, ΔS = 50.0 J mol^{-1} K^{-1}), in agreement with previously

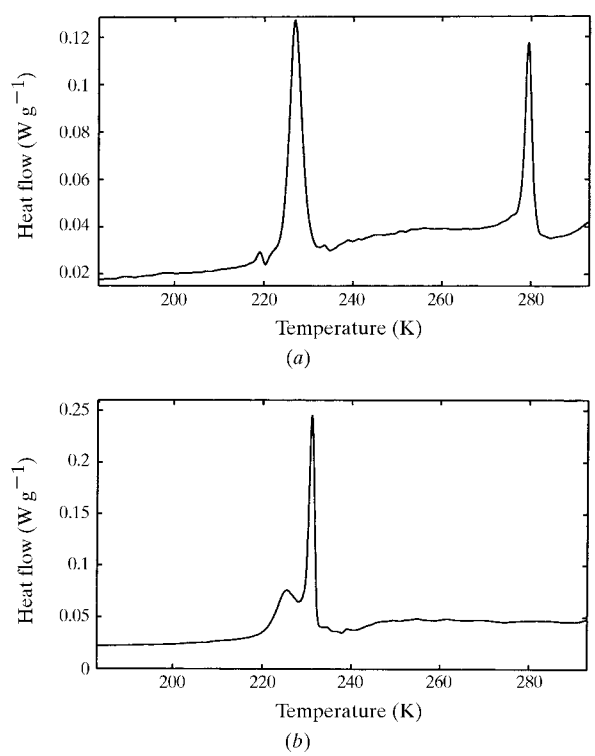

Fig. 2. Thermograms of the total heat flow (Gill *et al.*, 1993; Reading *et al.*, 1994), as measured by differential scanning calorimetry between 190 and 290 K for (*a*) TC and (*b*) TSi.

Table 1. *Experimental details*

	TSi295	TSi200	TC295	TC260	TC150
Crystal data					
Chemical formula	$Si[Si(CH_3)_3]_4$	$Si[Si(CH_3)_3]_4$	$C[Si(CH_3)_3]_4$	$C[Si(CH_3)_3]_4$	$C[Si(CH_3)_3]_4$
Chemical formula weight	320.87	320.87	304.79	304.79	304.79
Cell setting	Cubic	Cubic	Cubic	Cubic	Cubic
Space group	$Fm\bar{3}m$	$P2_13$	$Fm\bar{3}m$	$Pa\bar{3}$	$P2_13$
a (Å)	13.5218 (1)	13.17158 (6)	12.8902 (1)	12.7876 (1)	12.609 (3)
V (Å^3)	2472.3 (1)	2285.15 (2)	2141.8 (1)	2091.0 (1)	2005 (1)
Z	4	4	4	4	4
D_x (Mg m^{-3})	0.862	0.932	0.945	0.968	1.01
2θ range (°)	6.0–52.0	6.0–59.0	3.2–35.0	3.2–22.0	6.0–32.0
Step size, 2θ (°)	0.005	0.01	0.002	0.004	0.003
Counting time per step (s)	3.2	8.3	1.2–2.2	3.2	3.2–9.2
Radiation type	Synchrotron	Synchrotron	Synchrotron	Synchrotron	Synchrotron
Wavelength (Å)	1.14946 (2)	1.14946 (2)	0.82488 (2)	0.82488 (2)	0.82488 (2)
Temperature (K)	295	200	295	260	150

reported measurements (Murrill & Breed, 1971). On cooling, the DSC trace for TSi (Fig. 2*b*) displayed a second peak, which was not observed in heating runs. Tentatively, this may be ascribed to the presence of a second phase transition, which is obliterated on heating by the hysteresis of the transitions.

The solid-state ^{13}C NMR experiment on TC was carried out on a Bruker MSL 300 NMR spectrometer, corresponding to Larmor frequencies $\omega_0/2\pi = 75.5$ MHz (^{13}C) and $\omega_0/2\pi = 59.6$ MHz (^{29}Si). Details of the NMR experiment are described elsewhere (Helluy *et al.*, 1998). Isotropic chemical shifts $\delta(^{13}C)$ and $\delta(^{29}Si)$ are quoted with respect to $Si(CH_3)_4$.

For the X-ray powder diffraction experiments, the samples were sealed in glass capillaries of 0.7 mm diameter (Hilgenberg glass No. 50). High-resolution powder diffraction data were collected at several temperatures at beamline X3B1 at the National Synchrotron Light Source, Brookhaven National Laboratory (Table 1). For the low-temperature measurements, a closed-cycle helium cryostat was used. X-ray wavelengths were selected by a double Si(111) monochromator and they were calibrated with the NBS1976 alumina standard. The diffracted beam was analyzed with a Ge(111) crystal and detected with a Na(Tl)I scintillation counter with a pulse-height discri-

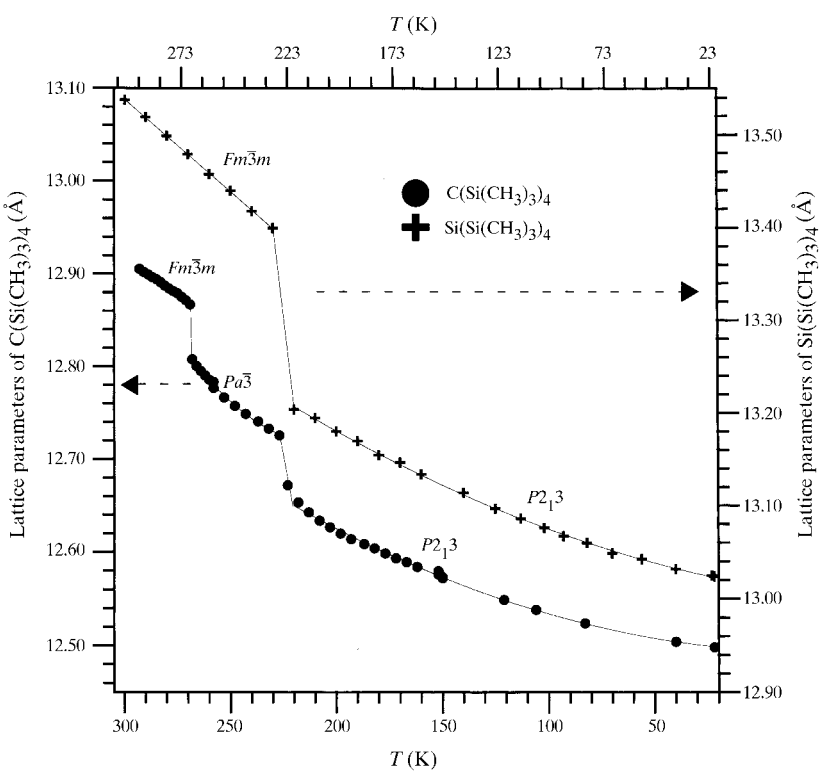

Fig. 3. Cubic lattice parameter as a function of temperature for TC and TSi. Note the offset of the two lattice-parameter scales.

minator in the counting chain. The intensity of the primary beam was monitored by an ion chamber. In this parallel beam geometry the resolution is determined by the analyzer crystal instead of by slits.

The temperature dependences of the lattice parameters of TC and TSi were monitored from 300 K to 20 K by repeatedly scanning the (222) reflection (Fig. 3). The wavelength used was 0.82488 (2) Å. The temperatures of the phase transitions thus obtained differ from those determined by DSC measurements by amounts between 2 K and 11 K, but they agree with the values obtained by NMR. We regard the values as determined by X-ray powder diffraction to be more accurate. Full powder patterns were taken for all phases. For TSi [wavelength 1.14946 (2) Å], X-ray scattering intensities were recorded at T = 295 K for 3.2 s at each 2θ in steps of 0.005° from 6.0 to 52° (Fig. 4*a*), and at T = 200 K for 8.3 s at each 2θ in steps of 0.01° from 6.0 to 59° (Fig. 4*b*). For TC [wavelength 0.82488 (2) Å], X-ray scattering was measured at T = 295 K for 1.2 s at each 2θ in steps of 0.002° from 3.2 to 22.0°, and for 2.2 s at each 2θ from 20.0 to 35.0° (Fig. 5*a*), at T = 260 K for 3.2 s at each 2θ in steps of 0.004° from 3.2 to 22.0° (Fig. 5*b*), and at T = 150 K for 3.2 s at each 2θ in steps of 0.003° from 6.0 to 18.0°, and for 9.2 s at each 2θ in steps of 0.003° from 18.0 to 32.0 (Fig. 5*c*). Samples were either spun or rocked around θ by several degrees (6–25°) during measurement to reduce crystallite-size effects.

The diffraction patterns at room temperature are characterized by a rapid fall-off of the diffracted intensity with increasing diffraction angle. Reflections could not be detected above $\sin\theta/\lambda \simeq 0.34$ Å^{-1} for either TSi or TC. Indexing of the powder patterns of TC and TSi at room temperature led to a face-centered cubic lattice with space group $Fm\bar{3}m$ or one of its subgroups. In the low-temperature phases the lattices are reduced to

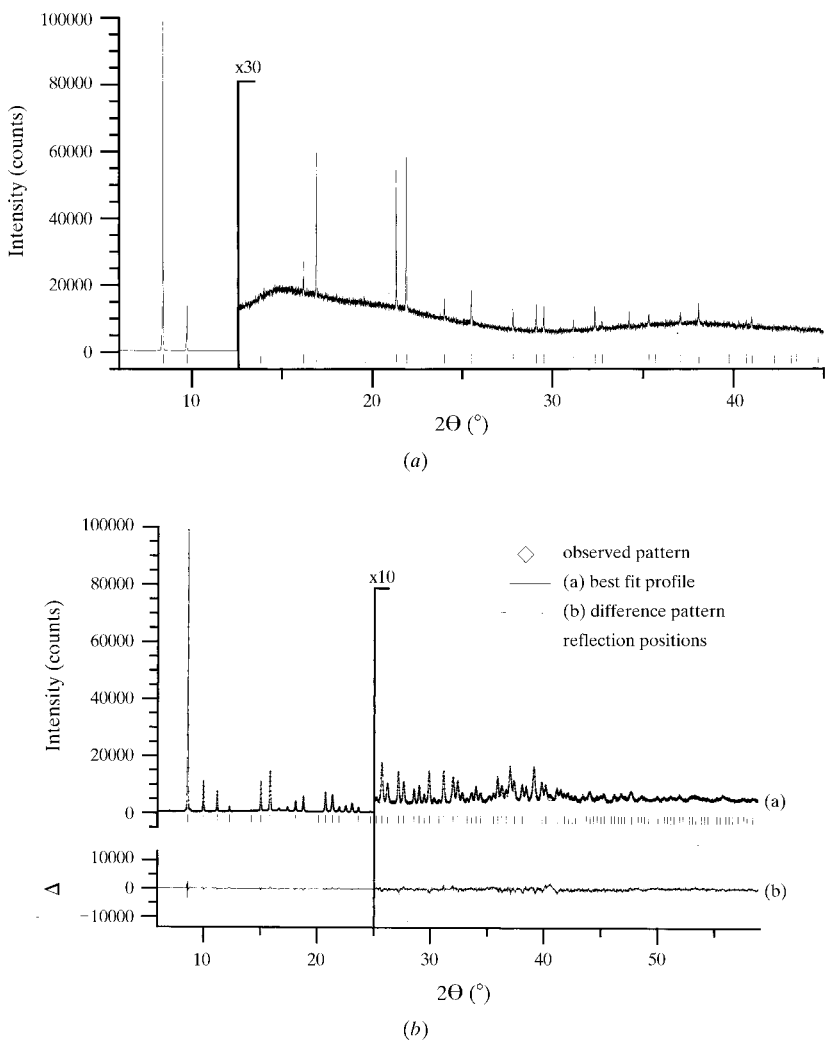

Fig. 4. (*a*) Scattered X-ray intensity for the high-temperature phase of TSi at T = 295 K as a function of diffraction angle 2θ. The wavelength was λ = 1.14946 (2) Å. The higher angle part starting at 12.5° 2θ is enlarged by a factor of 30. (*b*) Scattered X-ray intensity for the low-temperature phase of TSi at T = 200 K as a function of diffraction angle 2θ. Shown are the observed pattern (diamonds), the best Rietveld-fit profile in $Pa\bar{3}$ (line a), the difference curve between observed and calculated profiles (line b), and the reflection markers (vertical bars). The wavelength was λ = 1.14946 (2) Å. The higher angle part starting at 10° 2θ is enlarged by a factor of ten. The R values are R_p = 0.0515, R_{wp} = 0.0657, $R(F^2)$ = 0.1142.

primitive. The space group of the intermediate phase of TC could be determined unambiguously as $Pa\bar{3}$ from the observed extinction rules. For the low-temperature phases of TC and TSi, no extinctions could be found in the scattering and several possible space groups remained. Owing to the direct sub-supergroup relation

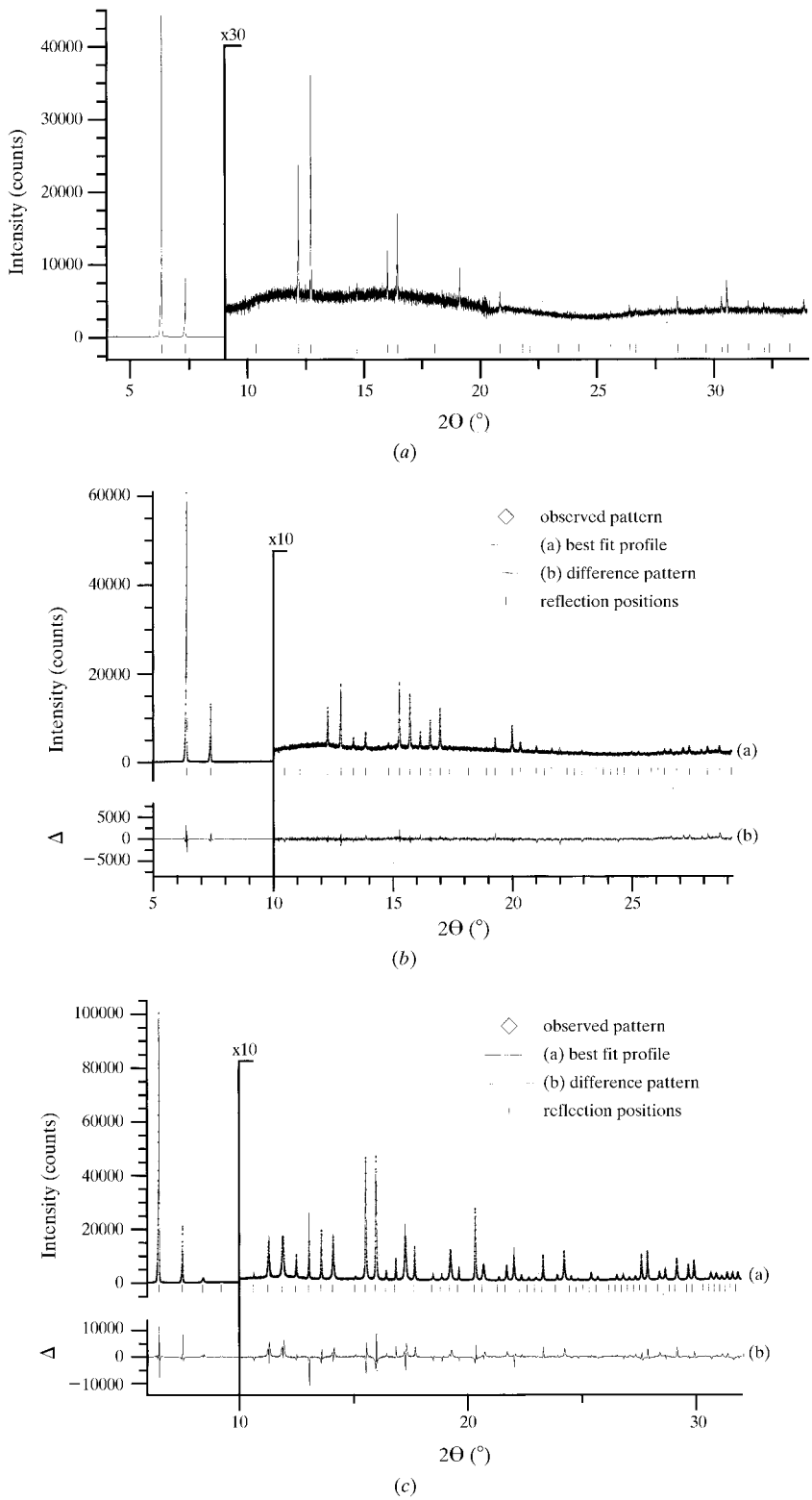

Fig. 5. (*a*) Scattered X-ray intensity for the high-temperature phase of TC at T = 295 K as a function of diffraction angle 2θ. The wavelength was λ = 0.82488 (2) Å. The higher angle part starting at 9° 2θ is enlarged by a factor of 30. (*b*) Scattered X-ray intensity for the intermediate phase of TC at T = 260 K as a function of diffraction angle 2θ. Shown are the observed pattern (diamonds), the best Rietveld-fit profile in $Pa\bar{3}$ (line a), the difference curve between observed and calculated profiles (line b), and the reflection markers (vertical bars). The wavelength was λ = 0.82488 (2) Å. The higher angle part starting at 10° 2θ is enlarged by a factor of 10. The R values are R_p = 0.0619, R_{wp} = 0.0838, $R(F^2)$ = 0.172. (*c*) Scattered X-ray intensity for the low-temperature phase of TC at T = 150 K as a function of diffraction angle 2θ. Shown are the observed pattern (diamonds), the best Rietveld-fit profile in $P2_13$ (line a), the difference curve between observed and calculated profile (line b), and the reflection markers (vertical bars). The wavelength was λ = 0.82488 (2) Å. The higher angle part starting at 10° 2θ is enlarged by a factor of ten. The R values are R_p = 0.1461, R_{wp} = 0.2029, $R(F^2)$ = 0.1778.

with $Pa\bar{3}$, $P2_13$ was chosen as the most likely candidate. The correctness of this assumption was confirmed by the refinement.

The peak profiles were determined by LeBail-type fits using the program *GSAS* (Larson & Von Dreele, 1994). The background was modeled manually, in combination with a four-term cosine series refined in *GSAS*. The peak profile was described by a pseudo-Voigt in combination with a special function that accounts for the asymmetry due to axial divergence (Thompson *et al.*, 1987; Finger *et al.*, 1994). The room-temperature phases displayed extremely sharp lines which could be described satisfactorily by a Lorentz-type profile. Upon cooling, both the Gaussian component of the peak and the total width increased considerably (Fig. 6).

For all measurements the integrated intensities and widths of all diffraction maxima were determined by least-squares fitting using the program *GUFI*5.0 (Dinnebier & Finger, 1998). For the room-temperature phases of TC and TSi, the widths of the maxima in the scattering are close to the resolution of the diffractometer (Figs. 7*a* and *b*). Below the phase transitions the scattering maxima are considerably broadened, but their widths also show a strong dependence on the directions of the scattering vectors, instead of a smooth dependence on the scattering angle only. For the low-temperature phase of TSi and the intermediate phase of TC, the variations of peak widths could be described by an anisotropic strain model, as recently developed by Stephens (1999). Only two additional parameters were required to describe the peak profiles, representing moments of the distribution of the lattice parameters.

The distribution of widths of the scattering maxima of the low-temperature phase of TC could not be described by this model. Therefore, we developed a model based on finite domain sizes (§3).

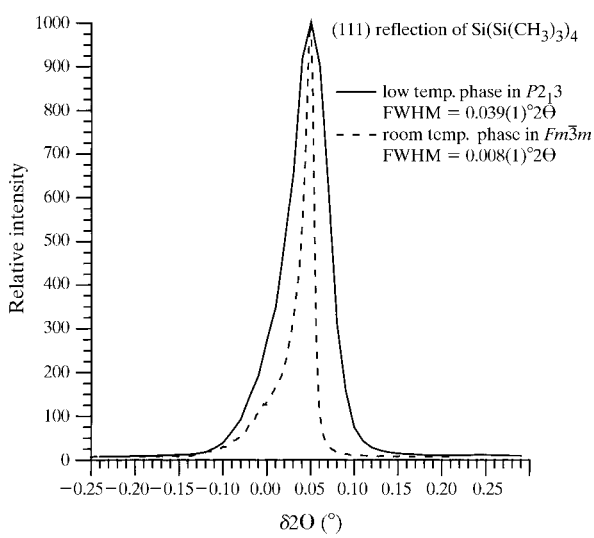

Fig. 6. Profiles of the (111) reflection of TSi at 295 and 200 K. Note the much larger width at the lower temperature.

A small trace of an unidentified additional phase was observed in one peak at 40.2° 2θ in the powder pattern of TSi. Some weak broad features suggest the presence of an amorphous fraction.

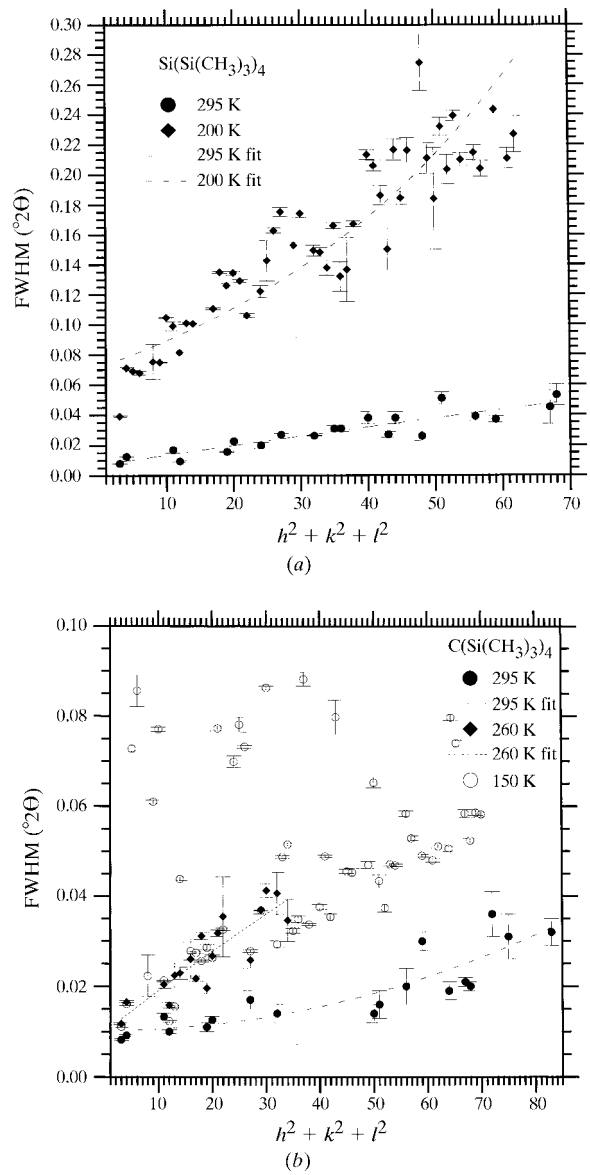

Fig. 7. Full width at half maximum (FWHM) as a function of $(h^2 + k^2 + l^2)$ for the two different phases of TSi at temperatures 295 K, and 200 K, respectively. The FWHM for the low-temperature phase shows more variation than FWHM for the high-temperature phase. The low-temperature phase of TSi shows strong broadening for all the peaks, but the deviations from the smooth curve can be described by the method of Stephens (1999). (*b*) Full width at half maximum (FWHM) as a function of $(h^2 + k^2 + l^2)$ for the three different phases of TC, at temperatures 295, 260 and 150 K, respectively. Whereas the FWHM for the high- and intermediate-temperature phases can be described by a smooth function of diffraction angle within the error limits, the distribution for the low temperature appears more complicated.

3. X-ray structure determination

3.1. *Room-temperature structures*

For the room-temperature structure, integrated intensities derived by single-peak fitting were used to test several structure models. Unobserved reflections were assigned the uncertainty of the weakest observable nearby peak and an intensity of half this uncertainty. Tables S1† and S2† list the intensities (and derived squared structure factor sums) of the room-temperature synchrotron data.

Refinements showed that the molecules are arranged in a cubic closed-packed (c.c.p.) array with space group $Fm\bar{3}m$. Since the crystallographic symmetry of the c.c.p. site is higher than the molecular symmetry, the molecules must be orientationally disordered. It appeared that our X-ray diffraction data can discriminate between a model with randomly oriented molecules and a model with disorder of the molecules over a few orientations. For dynamic disorder the former corresponds to free rotations of the molecules, whereas the latter reflects jumps between the various orientations. The scattering of the free-rotation model can be described by the sum of the scattering of a central atom (C or Si), a spherical shell with the scattering power of four Si atoms, and a spherical shell with the scattering power of 12 methyl groups (Bée, 1988). The shell radii were taken from the gas-phase studies of TC and TSi (Bartell *et al.*, 1970; Beagley *et al.*, 1988) and kept fixed during the refinement. Three variables (scale factor, overall isotropic displacement factor, and effective occupancy of the outer shell) were refined by the method of least squares leading to a best fit with $R(F^2)$ = 0.232 for TC and $R(F^2)$ = 0.255 for TSi. The deviation between the spherical shell form factor and the observed structure factors indicate that the molecular orientations must deviate significantly from a truly random orientation (Figs. 8*a* and *b*).

A disordered but non-random distribution of molecular orientations was modeled by a set of fractionally occupied sites. An initial structure model was determined in space group $Fm\bar{3}m$ by placing Si or C atoms at their appropriate distances from the central Si or C atom along different directions and allowing their site occupancy and positional parameters to vary. In this manner it was determined that atoms of the intermediate Si shell tended to be concentrated along directions close to ⟨120⟩, while atoms in the outer methyl-group shell tended to be concentrated along directions between ⟨111⟩ and ⟨100⟩. It was noted that such a distribution of sites can be obtained by rotation of the gas-phase TSi or TC molecule from a hypothetical ordered $F23$ structure [as given by Beagley *et al.* (1989)] by 45° around any ⟨100⟩ axis and reproducing this rotated molecule by the space group symmetry of $Fm\bar{3}m$. The 17-atom molecule represented by three atoms in $Fm\bar{3}m$ then becomes 12 orientations in $Fm\bar{3}m$ represented by five atoms, Si(0), Si(1), C(1), C(2) and C(3). These 12 orientations were not uniformly distributed in space but formed six pairs, each consisting of two similar orientations. The $R(F^2)$ of 0.21 for the rigid-rotation model of TSi indicated that

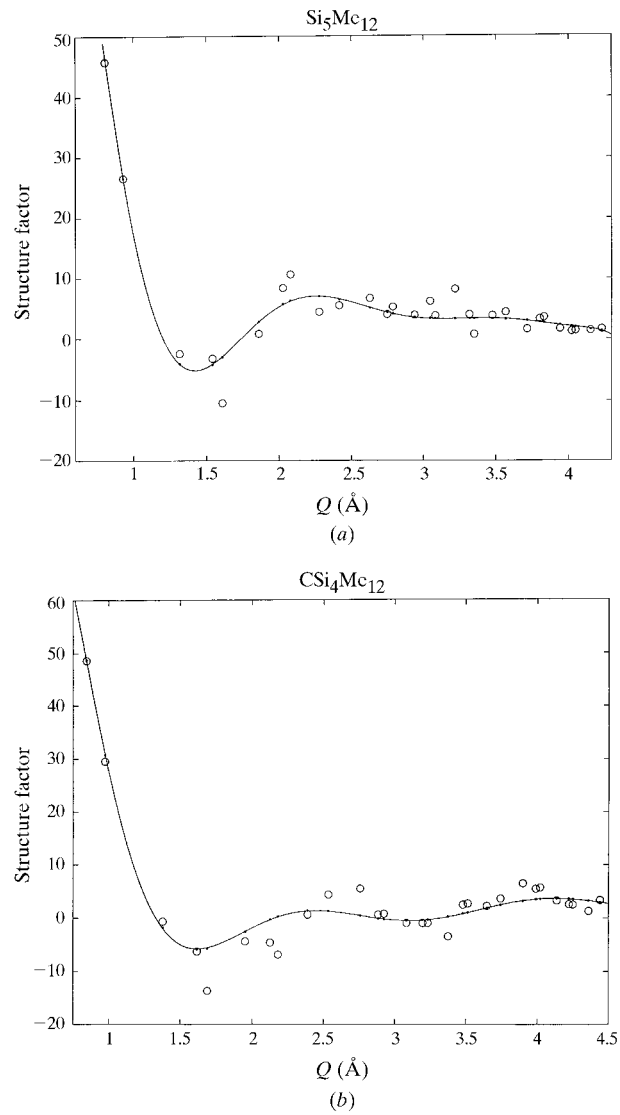

Fig. 8. Structure factors F(cal) of the random orientation model (individual dots) and structure factors F(obs) derived from the observed intensities (open circles), with signs from F(cal) for TSi (*a*) and TC (*b*). The F(cal) values have been connected by a fitted polynomial to emphasize their smooth variation. Note that the F(obs) values fall significantly off the smooth curves, indicating that the molecular orientations must deviate significantly from a truly random orientation.

† Tables S1 and S2 have been deposited. Supplementary data for this paper are available from the IUCr electronic archives (Reference: SE0261). Services for accessing these data are described at the back of the journal.

Table 2. *Positional parameters and occupancy*

(*a*) Positional parameters, U_i (Å^2 × 10^3), and occupancy of TSi (upper) and TC (lower) in $Fm\bar{3}m$ symmetry at 295 K; methyl-group occupancies, accounting for H-atom scattering, are constrained to be equal within each compound. (*b*) Positional parameters, U_i (Å^2 × 10^3), and occupancy of TSi at 200 K (top) and of TC at 260 K in $Pa\bar{3}$ (middle) and 150 K in $P2_13$ (bottom). The values of the temperature factor are constrained to be equal for C and Si atoms.

	x	*y*	*z*	U_i/U_e × 10^3	Occupancy
(*a*)					
Si(0)	0	0	0	203 (13)	1
C(0)	0	0	0	101 (13)	
Si(1)	0.028 (2)	0.086 (1)	0.154 (1)	Si(0)	1/16
	0.021 (3)	0.073 (2)	0.130 (2)	153 (25)	
C(1)	0.072 (3)	0.130 (3)	0.228 (4)	Si(0)	1.25 (5)/16
	0.067 (4)	0.126 (4)	0.225 (5)	C(0)	1.35 (8)/16
C(2)	0.113 (3)	0.168 (2)	*y*[C(2)]	Si(0)	2 × C(1)
	0.114 (3)	0.157 (2)	*y*[C(2)]	C(0)	2 × C(1)
C(3)	0.038 (1)	*x*[C(3)]	0.256 (2)	Si(0)	2 × C(1)
	0.039 (2)	*x*[C(3)]	0.240 (3)	C(0)	2 × C(1)
(*b*)					
Si(0)	0.0048	0.0048	0.0048	27.9 (5)	1.0
C(0)	0	0	0	265 (19)	1.0
C(0)	0	0	0	25.2 (9)	1.0
Si(1)	0.1072 (2)	0.1072 (2)	0.1072 (2)	27.9 (5)	1.0
	0.0847 (3)	0.0847 (3)	0.0847 (3)	317 (8)	0.5
	0.0881 (2)	0.0881 (2)	0.0881 (2)	25.2 (9)	1.0
Si(2)	0.0661 (2)	−0.1602 (2)	0.0078 (2)	27.9 (5)	1.0
	0.0352 (10)	−0.1415 (6)	−0.0073 (17)	317 (8)	0.5
	0.0548 (2)	−0.1425 (2)	−0.0005 (3)	25.2 (9)	1.0
C(11)	0.2452 (3)	0.0899 (5)	0.0877 (4)	119 (2)	1.5
	0.2172 (7)	0.0166 (13)	0.1032 (14)	174 (3)	0.75
	0.2380 (3)	0.0500 (7)	0.0666 (7)	25.2 (9)	1.5
C(21)	0.1134 (5)	−0.1936 (5)	0.1436 (4)	119 (2)	1.5
	0.1132 (21)	−0.1878 (15)	0.1119 (18)	174 (3)	0.75
	0.0966 (5)	−0.1785 (3)	0.1495 (4)	25.2 (9)	1.5
C(22)	−0.0361 (5)	−0.2510 (4)	−0.0396 (6)	119 (2)	1.5
	−0.0370 (13)	−0.2667 (7)	−0.0511 (11)	174 (3)	0.75
	−0.0417 (5)	−0.2425 (2)	−0.0548 (5)	25.2 (9)	1.5
C(23)	0.1905 (5)	−0.1711 (6)	−0.0710 (4)	119 (2)	1.5
	0.1467 (17)	−0.1474 (14)	−0.1070 (20)	174 (3)	0.75
	0.1905 (4)	−0.1418 (4)	−0.0846 (5)	25.2 (9)	1.5

the different molecular orientations produced by this particular rotation were only an approximation to an even more disordered distribution of molecular orientations.

Consequently, the rigid-rotation model was relaxed by allowing the positional parameters of the constituent atoms to vary (10 of the potential 12 atomic coordinates were freed, the remaining two being constrained by site symmetry). The relaxation of the atomic site coordinates, combined with relatively large displacement factors, has the effect of smearing out the electron density. In TC, one isotropic displacement factor was assigned to Si and another to C, while in TSi a single factor was used for all atoms. The site occupancies of the inner Si or C atoms were fixed at their molecular 1:4 ratios, while the occupancy of the three methyl groups were constrained to be equal, but adjusted to give the best fit to the intensity data. For both materials, displacement factors and effective methyl occupancies refined to essentially the same values as obtained in the spherical-shell models described above. The resulting *R*-factors for the relaxed TSi model are $R(F^2) = 0.046$ and $R_w(F^2) = 0.051$ for 29 observations, representing a total of 37 independent reflections. For the relaxed TC model, $R(F^2) = 0.059$ and $R_w(F^2) = 0.048$ for the same 29 observations, representing a total of 37 independent reflections. Tables S1 and S2 compare the observed and calculated square structure factors. Attempts of refinements in other space groups than $Fm\bar{3}m$ yielded very poor agreement with observed intensities.

Table 2(*a*) lists coordinates, occupancies and displacement factors of the atomic sites in the final refined models. Si(1) and C(1) are represented by 48 partially occupied sites, while C(2) and C(3) are each represented by 24 partially occupied sites. The low fractional site occupancies of ∼0.1 for Si and 0.2 for the methyl groups, and high displacement factors, yield relatively large errors in partial-atom locations.

The directions of the bonds between the central Si or C atom and the surrounding partially occupied atom

sites are conveniently represented on a stereographic projection. Fig. 9 shows the distribution of Si atoms and of methyl groups for TSi. TC results are not significantly different. The distribution of Si 'inner' shell atoms shows a broad maximum near ⟨110⟩, while the outer methyl-shell atoms are broadly distributed with a minimum around ⟨110⟩. This disorder with C(0)—Si bonds (nearly) in {100} planes is in agreement with the earlier prediction for the room-temperature phase of TC (Dereppe & Magill, 1972).

Table 3. *Rigid-body coordinates of a trimethylsilyl group with the origin located at the central Si(0)/C(0) atom*

The multipliers t_1 and t_2 for the two vectors needed to build the rigid body are equivalent to Si—Si and Si—C bond lengths

	t_1 = 2.34			t_2 = 1.89		
Si(1)	0	0	1	0	0	0
C(11)	0	0	1	$(2/3)^{1/2}$	$-(1/3)2^{1/2}$	1/3
C(12)	0	0	1	0	$(2/3)2^{1/2}$	1/3
C(13)	0	0	1	$-(2/3)2^{1/2}$	$-(1/3)2^{1/2}$	1/3

3.2. *Low-temperature structures*

Structure solution of the low-temperature structures of TC and TSi was attempted by direct methods using the program *SIRPOW* (Cascarano *et al.*, 1992). All attempts failed, using different sets of starting parameters. This can be understood in view of systematic overlap of peaks immanent for cubic symmetry.

Because of the similarity of the lattice parameters at high temperature and at low temperature, significant changes are not expected for the locations of the centers of gravity of the molecules. Assuming a fully ordered structure in space group $P2_13$, the molecules were placed at the origin with one of the bonds Si—Si(1) or C—Si(1) directed along the threefold ⟨111⟩ axis. Using space-group symmetry only, there are seven independent atoms with a total of 16 independent positional parameters. Unconstrained refinement of the positional parameters did not converge using different starting orientations of the molecule, which can be understood from the fact that large shifts of the atoms are required to account for small changes in the orientations of the molecules. For structure solution, two rigid bodies representing the two crystallographic independent trimethylsilyl groups were used (Table 3). This step reduced the number of refinable parameters to five, while keeping the tetrahedral angle of 109.47° between the two rigid bodies: three rotations and the average C/Si—Si(1) and Si(1)—methyl bond lengths. The initial values for the bond lengths Si—C 1.889 and Si—Si 2.361 Å were taken from the literature (Bartell *et al.*, 1970). The rotations can be described as follows: rotation of the entire TC or TSi molecule around ⟨111⟩, rotation of the trimethylsilyl group on the ⟨111⟩ axis about this axis, and rotation of the second trimethylsilyl group about the C—Si(2) or Si—Si(2) bond axis. The angle between the two trimethylsilyl groups was released at the final stage of the refinement process, but did not change significantly.

The structures of the low-temperature phase of TSi and TC (Fig. 10) were solved by stepwise release of intramolecular degrees of freedom. Further refinements were performed with the rigid-body constraints replaced by soft constraints on the bond lengths Si—C (2.36 ± 0.05 Å) and C—C (1.89 ± 0.05 Å). Owing to rather poor profile fits for TC, no convergence was reached in the free-parameter refinement for this compound and the coordinates derived from the rigid-body Rietveld refinement were used for bond length and angle calculations. For TSi, the refinement with soft constraints converged without large distortions of the 'rigid-body' molecule, improving the $R(F^2)$ factor by approximately 5 absolute %. Nevertheless, a difference of about 5 absolute % between the weighted profile R factor of the Le Bail and the Rietveld fits remained. Since most experimental sources of error could be excluded, the difference between observed and calculated patterns was attributed to the influence of the H atoms which account for 33% of the scattering power of the methyl groups. Although the position of the H atoms can

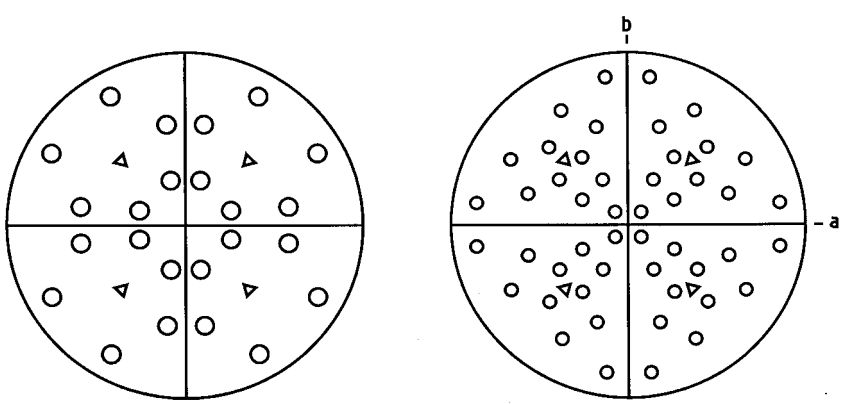

Fig. 9. Stereographic projection, showing the distribution of Si atoms (left) and of methyl groups (right) for TSi. The distribution of Si 'inner' shell atoms shows a broad maximum near ⟨110⟩, while the outer methyl-shell atoms are broadly distributed with a minimum around ⟨110⟩. This disorder with C(0)—Si bonds (nearly) in {100} planes is in agreement with the earlier prediction for the room-temperature phase of TC by Piret (Dereppe & Magill, 1972).

Table 4. *Selected intra- and intermolecular distances and angles of the ordered low-temperature structures of TC (rigid body refinement) and TSi (free refinement) and the intermediate phase of TC (rigid body refinement)*

Torsion angles are given as deviations from the staggered conformation (60°).

	$Si[Si(CH_3)_3]_4$ at 200 K	$C[Si(CH_3)_3]_4$ at 260 K	$C[Si(CH_3)_3]_4$ at 150 K
Distances (Å)			
C/Si(0)—Si(1), Si(2)	2.34, 2.32	1.88, 1.87	1.92
Si(1)—C(11)	1.85	1.92	1.97
Si(2)—C(2*x*)	1.91–1.95	1.91–1.93	1.88–2.02
C—C minimum intramolecular	2.91	2.88	3.21
C—C intermolecular	> 3.9	–	> 3.9
Angles (°)			
Si(1), C/Si(0), Si(2)	109.3	116.7	109.5
Si(2), C/Si(0), Si(2)	109.7	101.4	109.5
C/Si(0)/C(11), Si(1), C(11)	103.9, 114.6	108.6, 110.3	109.4, 109.5
C/Si(0)/C(2*x*), Si(2), C(2*x*)	101.8–112.7	97.5–134.7	105.9–113.2
Si(2), C/Si(0), Si(1), C(11)	13.7	18.8	20.3
Si(2), C/Si(0), Si(2), C(2*x*)	17.5 (average)	27.5 (average)	14.4 (average)

usually not be determined by powder-diffraction techniques, the contribution of H atoms to the profile is definitely measurable (*e.g.* Lightfoot *et al.*, 1993). It was not possible to include the positions of the H atoms in the refinement because of severe disorder. Therefore, the contribution of the H atoms to the scattering was described by increasing the occupation of the C atoms to values larger than 1. Refinement of this occupation resulted in an occupation of exactly 1.5, which is equivalent to nine instead of six electrons, accounting for the scattering power of the three H atoms of the methyl group. In order to avoid correlation between site-occupancy factor and temperature factor, the value for the site occupancy of the C atoms was then fixed to 1.5 for the following refinements. The final weighted profile (R_{wp} = 0.0657 for TSi, R_{wp} = 0.2029 for TC) converged to values close to that of the best Le Bail fit (R_{wp} = 0.0538 for TSi, R_{wp} = 0.1787 for TC; Figs. 4*b* and 5*c*). The refined Si—C bond lengths are higher than expected from the gas-phase studies, which can be attributed to the influence of the H atoms on the scattering of the methyl groups.

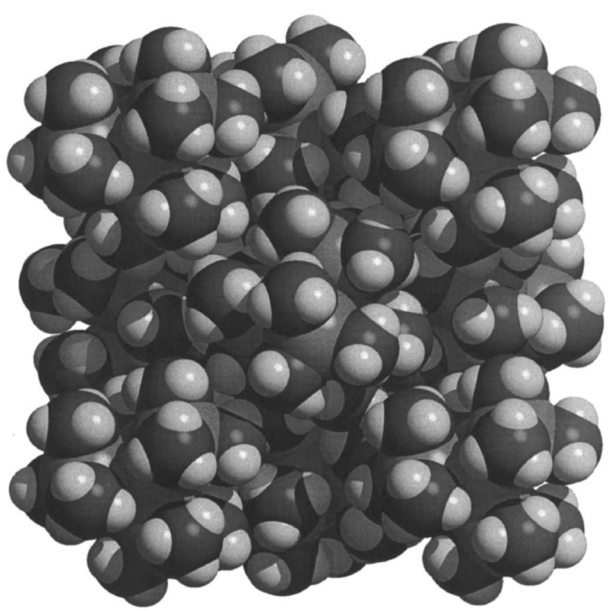

Fig. 10. Structure plot of the low-temperature phases TC and TSi in $P2_13$. The nesting of the methyl groups is optimized for close packing.

The crystal structure of the intermediate phase of TC could be directly derived from the corresponding structure of the low-temperature phase. The additional center of symmetry present in $Pa\bar{3}$ creates twofold disorder. The high quality of the powder diffraction pattern (Fig. 5*b*) allowed the refinement of individual atomic coordinates employing soft constraints only, confirming the correctness of the derived structural model. Atomic coordinates, displacement factors and selected intra- and intermolecular distances and angles are given in Tables 2 and 4.

The use of rigid bodies for the low-temperature structures was a crucial step at the beginning of the Rietveld refinement for two reasons. Firstly, the convergence radius of the isolated atoms was too small to allow for a successful refinement from random starting orientations of the molecule. Secondly, the strong anisotropy in the peak widths of TC did not allow the refinement of individual atomic positions even when the correct orientation of the molecule was used.

The low-temperature ($P2_13$) phase of TC exhibits a very unusual pattern of peak broadening *versus* diffraction order (open circles in Fig. 7*b*). It does not match the strain-broadening model (Stephens, 1999) which does apply to TSi in the same phase. One notes that the peaks are distributed over two classes: sharp and broad. The sharp peaks have widths comparable with those in the $Pa\bar{3}$ phase; furthermore, they generally correspond to peaks which are strong in the $Pa\bar{3}$ phase, *e.g.* (111), (200), (311), (320). The broad peaks have a FWHM of the order 0.08°, with no clear trend on diffraction order. This suggests some form of disorder, such that the spatial periodicities corresponding to

Table 5. *Possible orientations of the molecules in the unit cell of TC at low temperature, showing the separation of the statistically disordered molecules in the $Pa\bar{3}$ phase in two domains (labeled + and −) in the $P2_13$ phase*

Molecule center	$Pa\bar{3}$	$P2_13$ + domain	$P2_13$ − domain
(0, 0, 0)	$[111]$ or $[\bar{1}\bar{1}\bar{1}]$	$[111]$	$[\bar{1}\bar{1}\bar{1}]$
(1/2, 0, 1/2)	$[\bar{1}1\bar{1}]$ or $[11\bar{1}]$	$[\bar{1}1\bar{1}]$	$[11\bar{1}]$
(0, 1/2, 1/2)	$[\bar{1}\bar{1}1]$ or $[1\bar{1}1]$	$[\bar{1}\bar{1}1]$	$[1\bar{1}1]$
(1/2, 1/2, 0)	$[1\bar{1}\bar{1}]$ or $[\bar{1}11]$	$[1\bar{1}\bar{1}]$	$[\bar{1}11]$

broad peaks are correlated over a shorter range than the grain size.

It is possible to explain this observation by a model, based on finite-range orientational disorder within the low-temperature phase. First, recall that $Pa\bar{3}$ symmetry implies at least twofold disorder of the molecular orientations. In both $Pa\bar{3}$ and $P2_13$ the centers of the molecules form an f.c.c. lattice. In both phases, eight orientations are possible for the TC molecules, as defined by the vector $(\pm1, \pm1, \pm1)$ specifying the directions of one of the tetramethylsilyl groups. In $Pa\bar{3}$ symmetry one of two orientations is found at each site, related by an inversion center. When the sample is cooled into the $P2_13$ phase, that orientational disorder is lost, thus creating two possible domains which we will label + and −. Table 5 lists the orientations allowed at each site for each domain. While long-range order in the $P2_13$ phase would require the entire sample to choose either the + or the − orientations, it is reasonable to expect that a real sample will break up into domains with a characteristic size L.

The X-ray scattering intensity at wavevector $\mathbf{Q}$ depends on the instantaneous correlation function (Lovesey, 1984)

$$\sum_{\text{atoms } j,j'} \langle \exp(-i\mathbf{Q}.\mathbf{R}_j) f_j f_{j'} \exp(i\mathbf{Q}.\mathbf{R}_{j'}) \rangle = \sum_{\mathbf{R}} \langle A^*_{\mathbf{Q}}(0) A_{\mathbf{Q}}(\mathbf{R}) \rangle, \tag{1}$$

where f_j is the scattering amplitude of the atom j located at $\mathbf{R}_j$ and

$$A_{\mathbf{Q}}(\mathbf{R}) = \sum_j f_j \exp[i\mathbf{Q}.(\mathbf{R}_j - \mathbf{R})] \tag{2}$$

is the scattering amplitude from the unit cell centered at $\mathbf{R}$ (the sum runs over atoms $\mathbf{R}_j$ within the unit cell labeled by $\mathbf{R}$). If $A_{\mathbf{Q}}$ is the scattering amplitude per unit cell from a + domain, the amplitude from a − domain is $A^*_{\mathbf{Q}}$, because the two are related by an inversion. In the case that $\mathbf{Q}$ is close to a Bragg peak, we may replace $A_{\mathbf{Q}}$ by A_{hkl}. It is easy to see two limiting cases of the correlation function. As $R \to 0$,

$$\langle A^*_{\mathbf{Q}}(0) A_{\mathbf{Q}}(\mathbf{R}) \rangle \to \langle A^*_{\mathbf{Q}}(0) A_{\mathbf{Q}}(0) \rangle = |A_{hkl}|^2, \tag{3}$$

whereas for $R >> L$ the imaginary parts of the amplitude are uncorrelated, and so

$$\langle A^*_{\mathbf{Q}}(0) A_{\mathbf{Q}}(\mathbf{R}) \rangle \to (\text{Re } A_{hkl})^2. \tag{4}$$

A plausible correlation function is sketched in the inset of Fig. 11. It will give rise to a delta-function Bragg peak of intensity proportional to $(\text{Re } A_{hkl})^2$, plus a peak of width $\sim 1/L$ and an integrated intensity proportional to $|A_{hkl}|^2 - (\text{Re } A_{hkl})^2 = (\text{Im } A_{hkl})^2$, so that the total integrated intensity is proportional to $|A_{hkl}|^2$, as expected for a normal crystal with long-range order. Note that a disordered $Pa\bar{3}$ phase is described by the limit $L \to 0$, *i.e.* sharp Bragg peaks with intensities proportional to $(\text{Re } A_{hkl})^2$.

For the $P2_13$ phase in the present case, the delta-function, depending on the real part of A_{hkl}, is broadened by the finite grain size and strain which was already present in the $Pa\bar{3}$ phase. The broadest peaks which evidently arise from reflections with nearly imaginary amplitude, have a width of $\sim 0.08°$, implying that L is of the order of $\lambda/(2\pi d 2\theta) \simeq 100$ Å. Reflections with amplitudes intermediate between real and imaginary would produce composite peaks which could easily be mistaken for peaks of intermediate width. This model explains the tendency for peaks which are very weak or absent from the $Pa\bar{3}$ phase to be broad in the $P2_13$ phase: assuming that the structures of the two phases are sufficiently similar to give the same A_{hkl}, the disordered $Pa\bar{3}$ phase has Bragg intensities proportional to $(\text{Re } A_{hkl})^2$, which must be relatively larger than $(\text{Im } A_{hkl})^2$ to produce a sharp peak in the $P2_13$ phase. It is not possible to test this idea rigorously since most peaks are superpositions of multiple reflections (*hkl* and *khl* are generally not equivalent for either space group). However, there are several peaks which are uniquely

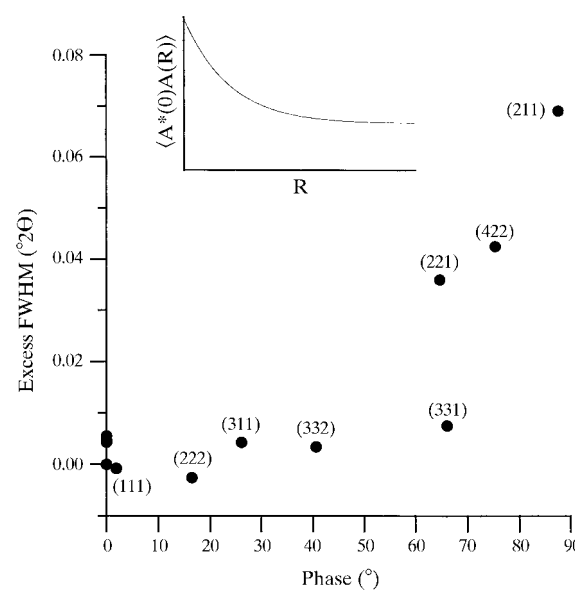

Fig. 11. Comparison of the calculated phase to the excess FWHM of several uniquely indexed diffraction peaks of TC in the $P2_13$ phase. The inset sketches a plausible correlation function.

indexed, and we can obtain estimates of their phase from the coordinates of the Rietveld refinement of the $P2_13$ diffraction data. The calculated phase is compared with the excess width of the diffraction peaks in Fig. 11, which shows a very strong correlation.

4. Lattice energy calculations

Calculations of the lattice energy showed the experimentally determined crystal structures of TSi and TC to be close to the structures of minimum energy. The same observation was made for the tetrahedral molecules $Zr(BH_4)_4$, $Zr(H_3B–CH_3)_4$, $Zr[H_3B–C(CH_3)_3]_4$ and $Zr\{H_3B–C[Si(CH_3)_3]_3\}_4$ (Schmidt & Englert, 1995; Welling *et al.*, 1995). The molecular geometry of TSi and TC was taken from electron diffraction data (Bartell *et al.*, 1970; Beagley *et al.*, 1988, 1989). The positions of the H atoms were calculated with the *Cerius*[2] program package (Molecular Simulations, 1997), applying the Dreiding force field (Mayo *et al.*, 1990) with modified parameters for silicon and carbon, in order to maintain the geometry of the Si/C fragment. The calculations result in torsion angles of θ(Si—Si—C—H) = 6° for TSi and θ(C—Si—C—H) = 5° for TC away from a staggered conformation of the methyl groups.

All lattice energy calculations were performed with the program *CRYSCA* (Schmidt & Englert, 1996; Schmidt & Kalkhof, 1998). This program performs lattice energy minimizations for rigid and flexible molecules in all space groups, and it allows the use of non-crystallographic symmetries. The atom–atom potential method (Pertsin & Kitaigorodsky, 1987) with a Buckingham-type potential was used with the potential parameters of Filippini & Gavezzotti (1993).

Since in TSi and TC the intramolecular forces are much stronger than the van der Waals forces between the molecules, the molecular geometry could be fixed during the packing calculations as a first approximation. The calculated packing did not change significantly when, in addition, the torsion angles were refined.

4.1. *Ordered $P2_13$ structures*

With fixed geometries of the molecules, the crystal packing can be described with only three variables: the lattice parameter a, the position of the molecule x(Si0) or x(C0), and the rotation φ_d around the ⟨111⟩ axes. For TSi the lattice energy minimizations converged at E = −78.1 kJ mol^{-1}. The optimized values of a = 13.126 Å, x = 0.0047, $\Delta\varphi_d$(calculated − observed) = 1.59° are close to the values determined by X-ray diffraction (Tables 1 and 2; Fig. 12). No other minimum with comparable or better energy was found. Similar results were derived for TC [E = −88.59 kJ mol^{-1}, a = 12.475, x = 0.0052 and $\Delta\varphi_d$(calculated − observed) = 0.12°].

Calculations with flexible molecules were performed by additionally releasing the torsion angles of the two crystallographically distinct trimethylsilyl groups. Even without applying intramolecular torsional potentials, the calculations led to a conformation that almost exactly reproduced the experimental findings. [For Si(1):

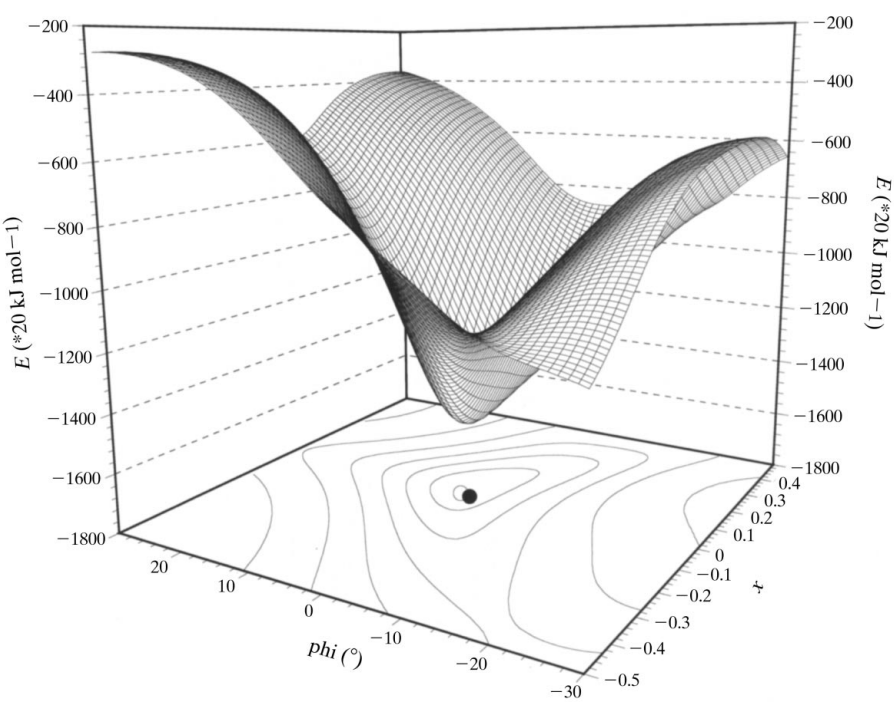

Fig. 12. The lattice energy of TSi in $P2_13$ from force field calculations. While the lattice parameter a is fixed to the experimental value, the position of the molecule x(Si0) along [111] axes, and the rotation φ_d around [111] axes are varied. Values of x = 0 and φ = 0° correspond to the experimental orientation of TSi (open circle), while x = 0.005 and φ = 1.59° denote the calculated values (filled circle).

calculated 11.2°, X-ray 13.7° (average); for Si(2): calculated 16.7°, X-ray 17.5° (average); electron diffraction: 11–14°.] This confirms that the orientation of the $SiMe_3$ groups is determined by both intra- and intermolecular forces..

4.2. *Pa*$\bar{3}$ *structures*

In *Pa*$\bar{3}$ the molecules are disordered around an inversion center. If, in each unit cell, two of the four molecules are inverted, the calculated lattice energy increases by 4.8 kJ mol^{-1} for TC and 6.0 kJ mol^{-1} for TSi. The higher energy for TSi explains why the *Pa*$\bar{3}$ symmetry is not adopted by TSi. The calculated energy difference for TC is larger than measured by DSC (2.01 kJ mol^{-1}). This indicates that the true local arrangement of the individual molecules is energetically more favorable than our simple static model for the disorder. The measured energy difference corresponds to an entropy increase of 1.06*R*.

4.3. *F23 structures*

In *F*23, $Z = 4$, the molecules incorporate their full 23(*T*) symmetry into the crystal structure. The hypothetical structures of TSi and TC in *F*23 were calculated by lattice energy minimizations. The resulting lattice energies are much higher than for the $P2_13$ structures ($\Delta E = +55.7$ kJ mol^{-1} for TSi, $\Delta E = +56.7$ kJ mol^{-1} for TC). Therefore, space group *F*23 can be ruled out.

4.4. *Fm*$\bar{3}$*m structures*

Assuming a completely statistical disorder the *Fm*$\bar{3}$*m* structure of TSi was calculated using a molecule which consisted of one fully occupied and 624 partially occupied atomic positions ($> 16 \times 10^6$ atom–atom interactions within 20 Å). The energy minimizations converged at a lattice energy of 48 kJ mol^{-1} above the $P2_13$ energy, with a lattice parameter of $a = 14.76$ Å. Both values do not fit the experimental data. This indicates that the local orientation of a molecule is neither purely statistical nor independent of the surrounding molecules. The orientations are strongly influenced by the orientation of their neighboring molecules, in accordance with the NMR experiments.

5. Discussion

The compounds tetrakis(trimethylsilyl)methane $C[Si(CH_3)_3]_4$ (TC) and tetrakis(trimethylsilyl)silane $Si[Si(CH_3)_3]_4$ (TSi) are isostructural in the low- and high-temperature phases, respectively, as is shown by X-ray scattering. Despite their similarities in chemistry and bond strengths [*e.g.* *F*(C—C) = 334 kJ mol^{-1}, *F*(Si—C) = 318 kJ mol^{-1}; Elschenbroich & Salzer, 1993], TC and TSi show substantially different behavior in their phase transitions and molecular dynamic properties.

5.1. *Phase transitions*

We have determined by X-ray scattering from powders that TSi shows a phase transition at $T = 225$ K from a disordered structure in space group *Fm*$\bar{3}$*m* towards a fully ordered structure in space group $P2_13$. In TC the transition from the disordered to the ordered structure occurs in two steps: at $T_1 = 268$ K from space group *Fm*$\bar{3}$*m* to space group *Pa*$\bar{3}$, and at $T_2 = 225$ K from space group *Pa*$\bar{3}$ to space group $P2_13$. The phase transitions represent large effects, as followed from the observed jumps in lattice parameters (Fig. 3).

All three phase transitions were also observed by DSC, albeit at slightly different temperatures (§2, Fig. 2). We believe the transition temperatures observed in the X-ray scattering experiments to be more accurate.

It is interesting to note that the sum of the changes in lattice parameters and the sum of the changes ΔH for the two transitions of TC are approximately equal to the corresponding changes at the single transition in TSi, indicating that the high- and low-temperature phases of TC and TSi are almost identical concerning the crystal packing and the free energy.

Solid-state MAS NMR clearly identifies the phase transition in TSi and the T_2 phase transition in TC (Helluy *et al.*, 1998). The T_1 phase transition could be identified as the onset of a small temperature-dependent shift of the peak position of the ^{13}C resonances of the methyl groups and the central carbon at $T \simeq 265$ K (Fig. 13). However, this effect is so small that by itself it could not have served as evidence for a phase transition. The failure to observe a clear effect for the T_2 phase transition in NMR can be explained by assumptions about the dynamical character of the disorder (see below).

5.2. *Crystal symmetry/order–disorder aspects*

The phase transitions are related to a change of the orientational order of the molecules. Upon cooling, the degree of structural order increases. Neglecting rotations of the methyl groups, the room-temperature phases were shown to contain at least sixfold orientational disorder, the intermediate phase of TC did have disorder over two orientations, and the low-temperature phases of TC and TSi were fully ordered. These features were determined by complete refinements of the crystal structures in all phases.

It has been shown that the experimentally observed structures were close to the structures corresponding to a minimum of the energy as obtained in calculations of the lattice energy. For the intermediate phase of TC evidence is given that an intermediate phase for TC in space group *Pa*$\bar{3}$ is energetically more favorable than for TSi.

The dynamical nature of the disorder can be derived from solid-state NMR (Helluy *et al.*, 1998). Thus, the following picture is obtained: the molecules show re-

orientational jumps of the whole molecule for TC and TSi and of the trimethylsilyl groups for TSi, even in the low-temperature phase. Extrapolation based on the Arrhenius plot of TC leads to reorientational jump rates of the order of 10 kHz for the intermediate phase. This high mobility of the molecule in combination with the occurrence of a single resonance signal clearly identifies the dynamic nature of the disorder for the intermediate temperature phase of TC.

Any non-random distribution of molecular orientations must be the result of interactions between neighboring molecules. In cubic close-packing the direction from one TSi or TC molecule to any of its 12 equivalent nearest neighbors is along the ⟨110⟩ directions of the cubic unit cell. The distribution of the outer methyl groups is almost uniform, except for a conspicuous absence in the ⟨110⟩ directions. That is, the molecular orientations observed at room temperature are those in which the outermost atoms point between, rather than directly at, neighboring molecules, thus improving molecular packing.

The lattice contractions in the low-temperature phases occur because of the nesting of the trimethylsilyl groups, as determined by X-ray powder diffraction (Fig. 10). The intramolecular crowding and consequently the amount of stress created in the molecular structure of TC is more severe than in the molecular structure of TSi due to the shorter C(0)—Si(1) bond length. This increased structural stress (or, equally, intramolecular steric crowding) finds its expression in different molecular dynamic properties as well as in different phase-transition properties of TC other than those observed for TSi.

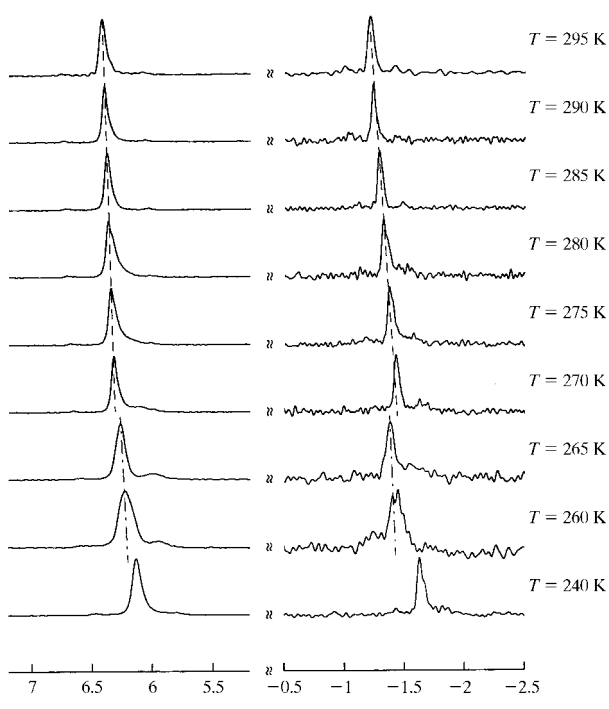

Fig. 13. ^{13}C CP/MAS NMR spectra of TC at various temperatures. Left column: ^{13}C methyl resonances; right column: ^{13}C resonances of the central carbon. The dashed lines are a guide to the eye for the temperature dependence of $\delta(^{13}C)$.

The nearest-neighbor distances between C atoms of the methyl groups of different molecules are greater than 3.9 Å for TC and TSi. Assuming a shell of disordered H atoms with a radius of 1 Å, this leads to a minimum distance of >1.9 Å between the molecules, which is close to the expected value of 2.1 Å (Table 3).

5.3. *Molecular symmetry*

Owing to the disorder, the molecular conformations in the high-temperature phases could not be determined from the X-ray experiments. A cooperate twist of 14° for TSi and 18° for TC of the trimethylsilyl groups from the reference (staggered) T_d structure was found by electron diffraction studies in the gas phase and could be confirmed by energy calculations. In the low-temperature phase this twist splits into two different groups, according to the two crystallographically distinct trimethylsilyl groups, with values of 13.7 and 17.5° for TSi, and 14.4 and 20.3° for TC, respectively, providing crystallographic evidence of molecular C_3 symmetry. The maximum deviation from the tetrahedral angle Si—Si(0)—Si in the low-temperature structure of TSi amounts to 0.2°. For the gas-phase structure, deviations of 1.6° have been reported from electron diffraction studies on TSi (Bartell *et al.*, 1970).

At T = 154 K the static ^{29}Si cross-polarization (CP) NMR spectrum of TSi (Fig. 14) displays an axially symmetric ^{29}Si chemical shielding tensor for the ^{29}Si resonance of the central Si atom, consistent with molecular C_3 symmetry. The NMR powder-pattern shape in the ^{29}Si–SiMe$_3$ spectral region is a superposition of two NMR powder patterns in relative 1:3 intensity for the Si$^{(1)}$Me$_3$ and Si$^{(2)}$Me$_3$ groups, respectively. This NMR powder-pattern shape gradually changes as a function of temperature, consistent with the dynamic properties of the low-temperature phase of TSi, as established by MAS NMR (Helluy *et al.*, 1998). Above the phase-transition temperature near T = 230 K, two narrow NMR powder patterns with a mixed Gaussian–Lorentzian lineshape are observed, one for the SiMe$_3$ groups (less shielded) and one for the central Si atom (more shielded). Only minor intrinsic temperature shifts are observed on further heating to T = 293 K. This fairly abrupt change of static ^{29}Si NMR powder-pattern shape near the phase-transition temperature can be rationalized in two different ways. One possibility would be preservation of molecular C_3 symmetry in the high-temperature phase of TSi, combined with an abrupt increase in molecular reorientation rates at increasing

temperatures to yield rapid (on the 10^3 Hz time scale of the ^{29}Si chemical shielding tensor) *and* isotropic molecular reorientation. The second, more likely, explanation is a change of molecular symmetry from C_3 to T on going to the high-temperature phase of TSi (plus a probably less abrupt increase in molecular reorientation rates at increasing temperatures).

As for TSi, the ^{29}Si–SiMe$_3$ spectral region of TC at low temperatures (Fig. 15) represents a superposition of the two ^{29}Si chemical-shielding NMR powder patterns for the two distinct types of Si$^{(1)}$Me$_3$ and Si$^{(2)}$Me$_3$ groups per molecule for the low-temperature phase. In the temperature range between T = 230 and 295 K, a single narrow ^{29}Si resonance of mixed Gaussian–Lorentzian shape is observed for both the intermediate and the high-temperature phase of TC. Again, it seems reasonable to ascribe the change in spectral ^{29}Si NMR line shape to a change in molecular symmetry from C_3 to T for the intermediate-temperature phase.

5.4. *Comparison with other quasispherical structures*

Several analogies between TC, TSi and C_{60} exist. The median distance of the central atom to the outer C atoms (3.57 Å for TSi and 3.1 Å for TC) is similar to the radius of the C_{60} molecule (3.55 Å; Chow *et al.*, 1992). For C_{60} and TC the transition from the high-temperature phase to the 'neighboring' low-temperature phase proceeds from $Fm\bar{3}m$ to $Pa\bar{3}$. The high molecular rigidity and the molecular inversion symmetry of C_{60} does not necessitate further reduction of space-group symmetry in order to arrive at a fully ordered structure, while the less rigid symmetric moieties of TC and TSi in their low-temperature phases proceed to space group $P2_13$, in which a fully ordered structure is possible.

The cage-like molecule of adamantane has tetrahedral symmetry (T_d; Norman & Schmitkons, 1965; Amoureux *et al.*, 1980). At 209 K, adamantane undergoes a phase transition from a twofold disordered phase in space group $Fm\bar{3}m$ at room temperature to an ordered low-temperature phase in space group $P\bar{4}2_1c$. At room temperature the less spherical adamantane molecule shows twofold disorder, TC and TSi show at least sixfold disorder, whereas the C_{60} molecule is nearly free rotating, while, at low temperature, adamantane, TC and TSi are ordered, the C_{60} molecule still shows twofold disorder.

The extremely small FWHM and strong intensity of the lowest angle peak of the room-temperature phases suggests the use of these materials as standards for the

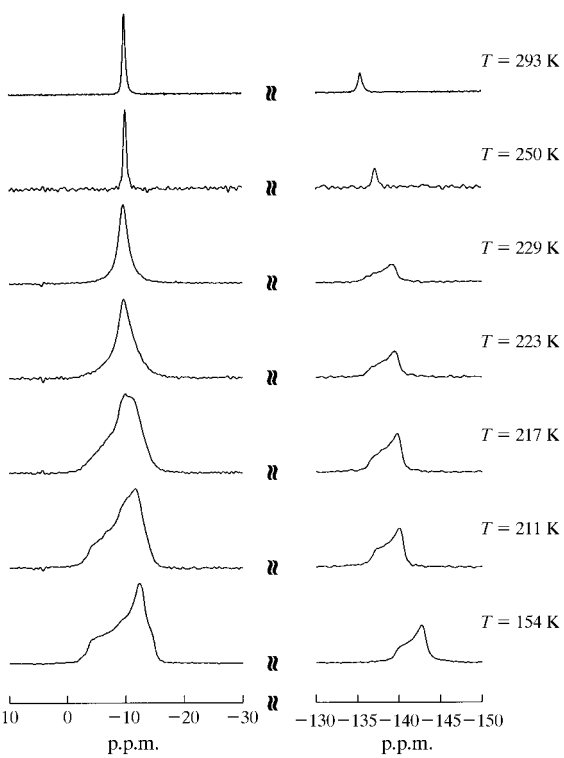

Fig. 14. Static ^{29}Si CP NMR spectra of TSi at various temperatures. The NMR powder pattern at −140 p.p.m. corresponds to the central Si atom, whereas the NMR powder pattern at −10 p.p.m. corresponds to the four outer Si atoms.

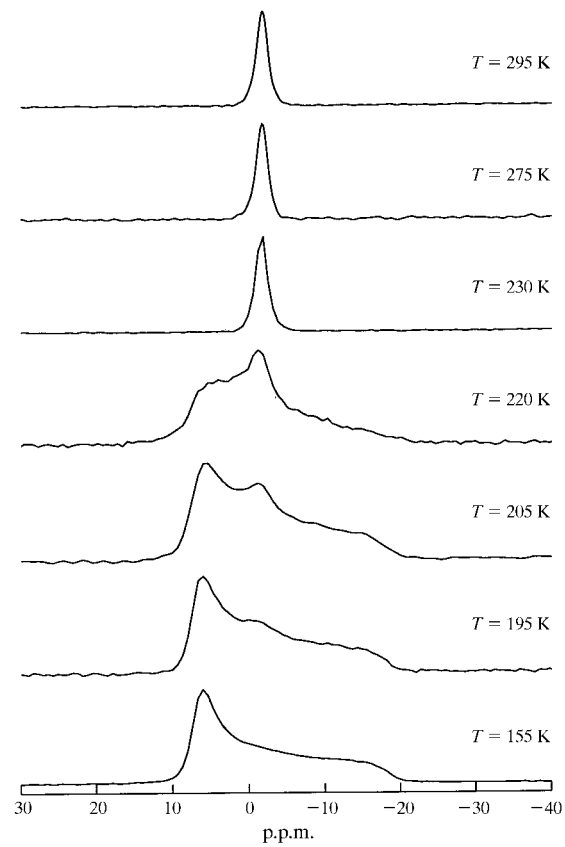

Fig. 15. Static ^{29}Si CP NMR spectra of TC at various temperatures.

determination of instrumental parameters of powder diffractometers, such as resolution and asymmetry due to axial divergence.

We are grateful to Sandrine Guinot from Rhône-Poulenc Rorer for carrying out the DSC measurements. Research was carried out in part at the National Synchrotron Light Source at Brookhaven National Laboratory, which is supported by the US Department of Energy, Division of Materials Sciences and Division of Chemical Sciences. The SUNY X3 beamline at NSLS is supported by the Division of Basic Energy Sciences of the US Department of Energy under Grant No. DE-FG02-86ER45231. PWS was partially supported by the National Science Foundation under grant DMR-95-01325. Financial support by the Deutsche Forschungsgemeinschaft (DFG) and the Fonds der Chemischen Industrie is gratefully acknowledged. We thank G. Fritz, Karlsruhe, for the donation of the TC sample.

References

Aliev, A. E., Harris, K. D. M. & Apperley, D. C. (1993). *J. Chem. Soc. Chem. Commun.* pp. 251–253.

Aliev, A. E., Harris, K. D. M., Apperley, D. C. & Harris, D. M. (1994). *J. Solid State Chem.* **110**, 314–320.

Amoureux, J. P., Bée, M. & Damien, J. C. (1980). *Acta Cryst.* B**36**, 2636–2642.

Bartell, L. S., Clippard, F. B. Jr & Boates, T. L. (1970). *Inorg. Chem.* **9**, 2436–2439.

Beagley, B., Pritchard, R. G. & Titiloye, J. O. (1988). *J. Mol. Struct.* **176**, 81–87.

Beagley, B., Pritchard, R. G. & Titiloye, J. O. (1989). *J. Mol. Struct.* **212**, 323–324.

Bée, M. (1988). *Quasielastic Neutron Scattering. Principles and Applications in Solid State Chemistry, Biology and Materials Science.* Bristol and Philadelphia: Hilger.

Bürger, H. & Goetze, U. (1968). *Angew. Chem.* **80**, 192–193.

Cascarano, G., Favia, L. & Giacovazzo, C. (1992). *J. Appl. Cryst.* **25**, 310–317.

Chow, P. C., Jiang, X., Reiter, G., Wochner, P., Moss, S. C., Axe, J. D., Hanson, J. C., McMullan, R. K., Meng, R. L. & Chu, C. W. (1992). *Phys. Rev. Lett.* **69**, 2943–2946.

Dereppe, J. M. & Magill, J. H. (1972). *J. Phys. Chem.* **76**, 4037–4039.

Dinnebier, R. E. & Finger, L. (1998). *Z. Kristallogr.* Suppl. 15, 148.

Elschenbroich, C. & Salzer, A. (1993). *Organometallchemie.* Stuttgart: B. G. Teubner.

Filippini, G. & Gavezzotti, A. (1993). *Acta Cryst.* B**49**, 868–880.

Finger, L. W., Cox, D. E. & Jephcoat, A. P. (1994). *J. Appl. Cryst.* **27**, 892–900.

Gill, P. S., Sauerbrunn, S. R. & Reading, M. (1993). *J. Therm. Anal.* **40**, 931–939.

Gilman, H. & Smith, C. L. (1964*a*). *J. Am. Chem. Soc.* **86**, 1454.

Gilman, H. & Smith, C. L. (1964*b*). *Inorg. Chem.* **32**, 2694–2698.

Haaland, A., Shorokhov, D. J., Strand, T. G., Kouvetakis, J. & O'Keeffe, M. (1997). *Inorg. Chem.* **36**, 5198–5201.

Haaland, A., Sokolov, V. I., Volden, H. V., Kühner, S. & Weidlein, J. (1996). *J. Organomet. Chem.* **524**, 285–287.

Heine, A., Herbst-Irmer, R., Sheldrick, G. M. & Stalke, D. (1993). *Inorg. Chem.* **32**, 2694–2698.

Helluy, X., Kümmerlen, J. & Sebald, A. (1998). *Organometallics.* In the press.

Iroff, L. D. & Mislow, K. (1978). *J. Am. Chem. Soc.* **100**, 2121–2126.

Klinkhammer, K. W., Kühner, S., Regelmann, B. & Weidlein, J. (1995). *J. Organomet. Chem.* **496**, 241–243.

Kuivila, H. G. & DiStefano, F. V. (1976). *J. Organomet. Chem.* **122**, 171–186.

Larson, A. C. & Von Dreele, R. B. (1994). *GSAS – General Structure Analysis System.* Report LAUR 86–748. Los Alamos National Laboratory, USA. (Available by anonymous FTP from mist.lansce.lanl.gov.)

Lightfoot, P., Metha, M. A. & Bruce, P. G. (1993). *Science*, **262**, 883–885.

Lovesey, S. W. (1984). *Theory of Neutron Scattering from Condensed Matter.* Oxford University Press.

Matsunaga, P. T., Kouvetakis, J. & Groy, T. L. (1995). *Inorg. Chem.* **34**, 5103–5104.

Mayo, S. L., Olafson, B. D. & Goddard, W. A. III (1990). *J. Phys. Chem.* **94**, 8897–8909.

Merker, R. L. & Scott, M. J. (1964). *Acta Cryst.* **17**, 315.

Molecular Simulations (1997). *Cerius*^{2}. Version 3.5. Molecular Simulations, San Diego, California, USA.

Murrill, E. & Breed, L. W. (1971). *Inorg. Chem.* **10**, 641–643.

Norman, C. E. & Schmitkons, D. L. (1965). *Acta Cryst.* **18**, 764.

Parsonage, N. G. & Staveley, L. A. K. (1978). *Disorder in Crystals.* Oxford: Clarendon Press.

Pertsin, A. J. & Kitaigorodsky, A. I. (1987). *The Atom–Atom Potential Method.* Berlin/Heidelberg/New York: Springer-Verlag.

Reading, M., Luget, A. & Wilson, R. (1994). *Thermochim. Acta*, **238**, 295–307.

Schmidt, M. U. & Englert, U. (1995). *Z. Krist.* Suppl. 9, 95.

Schmidt, M. U. & Englert, U. (1996). *J. Chem. Soc. Dalton Trans.* pp. 2077–2082.

Schmidt, M. U. & Kalkhof, H. (1998). *CRYSCA. Program for Crystal Structure Calculations.* Clariant GmbH, Frankfurt am Main, Germany.

Stephens, P. W. (1999). *J. Appl. Cryst.* **32**, 281–289.

Thompson, P., Cox, D. E. & Hastings, J. B. (1987). *J. Appl. Cryst.* **20**, 79–83.

Welling, U., Paetzold, P. & Englert, U. (1995). *Inorg. Chim. Acta*, **231**, 175–180.